

Dynamics of thin-film spin-ij transistors with perpendicular source-drain magnetizations

Xuhui Wang and Gerrit E. W. Bauer

Kavli Institute of NanoScience, Delft University of Technology, 2628 C J Delft, The Netherlands

Axel Homan

Materials Science Division and Center for Nanoscale Materials,
Argonne National Laboratory, Argonne, Illinois 60439, USA

(dated: February 8, 2022)

A "spin-ij transistor" is a lateral spin valve consisting of ferromagnetic source drain contacts to a thin-film normal metal island with an electrically insulating ferromagnetic base contact on top. We analyze the dc-current-driven magnetization dynamics of spin-ij transistors in which the source-drain contacts are magnetized perpendicularly to the device plane by magnetoelectronic circuit theory and the macrospin Landau-Lifshitz-Gilbert equation. Spin-ij scattering and spin pumping effects are taken into account. We find a steady-state rotation of the base magnetization at GHz frequencies that is tuneable by the source-drain bias. We discuss the advantages of the lateral structure for high-frequency generation and actuation of nanomechanical systems over recently proposed nanopillar structures.

I. INTRODUCTION

Current induced magnetization excitation by spin-transfer torque^{1,2} attracts considerable attention because of potential applications for magnetoelectronic devices. The prediction of current-induced magnetization reversal has been confirmed experimentally in multilayers structured into pillars of nanometer dimensions.^{3,4,5,6} The devices typically consist of two ferromagnetic layers with a high (fixed layer) and a low coercivity (free layer), separated by a normal metal spacer. The applied current flows perpendicular to the interfaces. Often magnetic anisotropies force the magnetizations into the plane of the magnetic layers. Recently a number of theoretical proposals pointed out interesting dynamics when the magnetization of one of the layers is oriented perpendicular to the interface planes.^{7,8,9}

Fundamental studies of charge and spin transport have also been carried out in thin-film metallic conductors structured on top of a planar substrate.^{10,11,12,13,14,15} The advantages compared to pillar structures are the flexible design and the relative ease to fabricate multi-terminal structures with additional functionalities such as the spin-torque transistor.¹⁶ The easy accessibility to microscopic imaging of the structure and magnetization distribution should make the lateral structure especially suitable to study current-induced magnetization dynamics. Previous studies focused on the static (dc) charge transport properties, but investigations of the dynamics of laterally structured devices are underway.^{17,18} Recently, non-local magnetization switching in a lateral spin valve structure has been demonstrated.¹⁹ In the present paper we investigate theoretically the dynamics of a lateral spin valve consisting of a normal metal film that is contacted by two magnetically hard ferromagnets. As sketched in Fig. 1, a (nearly) circular and magnetically soft ferromagnetic film is assumed deposited on top of the normal metal to form a spin-ij transistor.²⁰ We concentrate on a configuration in which the magnetization direction of the source-drain contacts lies perpendicular to the plane of the magnetization of the third (free) layer. This can be realized either by making the contacts from a material that has a strong crystalline magnetic anisotropy forcing the magnetization out of the plane, such as Co/Pt multilayers,²¹ or by growing the source/drain ferromagnetic contacts into deeply etched grooves to realize a suitable aspect ratio. In such a geometry, the magnetization of the free layer precesses around the demagnetizing field that arises when the magnetization is forced out of the plane by the spin-transfer torque, as has been discussed in Refs. 7,8,9. Therefore, as long as the out-of-plane magnetization of the free layer remains small, the free layer magnetization will always stay almost perpendicular to the source and drain magnetizations. In the present article we analyze in depth the coupled charge-spin-magnetization dynamics in such current-biased thin-film "magnetic fans" and point out the differences and advantages compared to the perpendicular pillar structures. A convenient and accurate tool to compute the dynamic properties of our device is the magnetoelectronic circuit theory for charge and spin transport²⁰ coupled to the Landau-Lifshitz-Gilbert equation in the macrospin model. We include spin-ij scattering in normal and ferromagnetic metals and the spin-pumping effect.^{22,23}

The article is organized as follows: In Section II, we briefly review the Landau-Lifshitz-Gilbert equation including the current driven and spin-pumping torques that can be derived by circuit theory. In Section III, the specific results for our "magnetic fan" are presented. The potential applications will be discussed in Section IV. Section V is devoted to the conclusion.

II. FORMALISM

We are interested in the magnetization dynamics of the soft ferromagnetic island (i.e., composed of perm alloy) on top of the normal metal as sketched in the Fig. 1. The Landau-Lifshitz-Gilbert (LLG) equation in the macro-spin model, in which the ferromagnetic order parameter is described by a single vector \mathbf{M} with constant modulus M_s , appears to describe experiments of current-driven magnetization dynamics well,²⁴ although some open questions remain.²⁵ Micromagnetic calculations of the perpendicular magnetization configuration in the pillar structure suggest a steady precession of the magnetization.⁸ The LLG equation for isolated ferromagnets has to be augmented by the magnetization torque \mathbf{L} that is induced by the spin accumulation in proximity of the interface as well as the spin pumping:

$$\frac{1}{\gamma} \frac{d\mathbf{m}}{dt} = \mathbf{m} \times \mathbf{H}_{\text{eff}} + \frac{\gamma_0}{M_s} \mathbf{m} \times \frac{d\mathbf{m}}{dt} + \frac{1}{V M_s} \mathbf{L} \quad (1)$$

where γ is the gyromagnetic constant, $\mathbf{m} = \mathbf{M}/M_s$ and \mathbf{H}_{eff} is the magnetic field including demagnetizing, anisotropy or other external fields. γ_0 is the Gilbert damping constant and V is the volume of the isolated bulk magnet.

$$\mathbf{L} = \mathbf{m} \times (\mathbf{I}_s^{(p)} + \mathbf{I}_s^{(b)}) \times \mathbf{m};$$

where $\mathbf{I}_s^{(p)}$ and $\mathbf{I}_s^{(b)}$ denote the pumped²² and bias-driven^{1,2} spin currents leaving the ferromagnet, respectively, and the vector products project out the components of the spin current normal to the magnetization direction.

In magnetoelectronic circuit theory a given device or circuit is split into nodes and resistors. In each node a charge potential and spin accumulation is excited by a voltage or current bias over the entire device that is connected to reservoirs at thermal equilibrium or by spin pumping. The currents are proportional to the chemical potential and spin accumulation differences over the resistors that connect the island to the nodes. The Kirchhoff rules representing spin and charge conservation close the system of equations that govern the transport. In the following we assume that the ferromagnetic layer thickness is larger than the magnetic coherence length $\ell_c = \hbar/k_F^{\uparrow} - k_F^{\downarrow}$ in terms of the majority and minority Fermi wave numbers that in transition metal ferromagnets is of the order of Angstroms.

Let us consider a ferromagnet-normal metal (F/N) interface in which the ferromagnet is at a chemical potential μ_0^F and spin accumulation $\mu_s^F \mathbf{m}$ (with magnetization direction \mathbf{m}), whereas the normal metal is at μ_0^N and spin accumulations. The charge current (in units of Ampere) and spin currents (in units of Joule), into the normal metal are²⁶

$$I_c = \frac{e}{2h} [2g(\mu_0^F - \mu_0^N) + pg_s^F - pg_m^N] \quad (2)$$

$$\begin{aligned} I_s^{(b)} &= \frac{g}{8} [2p(\mu_0^F - \mu_0^N) + \mu_s^F (1 - r) - \mu_s^N] \\ &\quad - \frac{g}{8} r s - \frac{g}{8} i(s - m) \end{aligned} \quad (3)$$

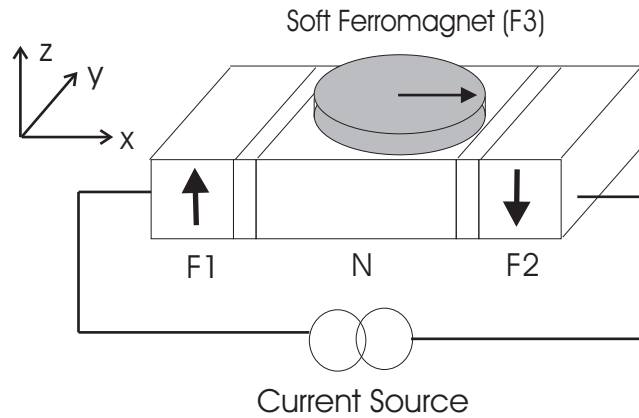


FIG. 1: The model system consists of hard-magnetic source and drain contacts (F1 and F2) with antiparallel magnetizations perpendicular to the plane. On the top of the normal metal N, a soft ferromagnetic film (F3) is deposited with a slightly elliptical shape. The quantization direction, i.e., z-axis, is chosen parallel to the magnetization of the source and the drain.

where μ_0^F and μ_0^N are the chemical potentials in the ferromagnets and normal metal, respectively. g'' ; $g^\#$ are the dimensionless spin dependent conductances with polarization $p = (g'' - g^\#)/(g'' + g^\#)$ and total contact conductance $g = g'' + g^\#$. In the Landauer-Buttiker formalism

$$g''(\#) = M \sum_{nm} r_{n(\#)}^{nm} r_{m(\#)}^{nm} \quad (4)$$

where M is the total number of channels and $r_{n(\#)}^{nm}$ is the reflection coefficient from mode m to mode n for spin up (down) electrons. The spin transfer torque is governed by the complex spin-mixing conductance $g''^\#$, given by²⁶

$$g''^\# = M \sum_{nm} r_n^{nm} (r_\#^{nm})^* ; \quad (5)$$

introduced in Eq. (3) in terms of its real and imaginary part as $\text{Re } g''^\# = g$ and $\text{Im } g''^\# = g_i$. All conductance parameters can be computed from first principles as well as fitted to experiments.

Slonczewski's spin transfer torque can then be written as

$$\mathbf{m} \times \frac{d\mathbf{m}}{dt} = \frac{g}{8} \mathbf{r} [\mathbf{s} \cdot (\mathbf{s} - \mathbf{m})\mathbf{m}] + \frac{g_i}{8} \mathbf{i} (\mathbf{s} - \mathbf{m}) ; \quad (6)$$

The spin-pumping current is given by²²

$$I_s^{(p)} = \frac{h}{8} g \mathbf{r} \mathbf{m} \cdot \frac{d\mathbf{m}}{dt} + \mathbf{i} \frac{d\mathbf{m}}{dt} \cdot \quad (7)$$

We consider for simplicity the regime in which the spin- $\uparrow\downarrow$ diffusion length l_{sf}^N in the normal metal node is larger than the size of the normal metal region.¹² Charge and spin currents into the normal metal node are then conserved such that²⁰

$$\sum_i I_{c,i} = 0 \quad (8)$$

$$\sum_i I_{s,i}^{(p)} + I_{s,i}^{(b)} = I_s^{sf} ; \quad (9)$$

where we introduce a leakage current due to the spin- $\uparrow\downarrow$ scattering $I_s^{sf} = g_{sf} s = 4$ and $g_{sf} = \hbar \rho_{\text{DOS}} V_N = \frac{N}{s_{sf}}$ is the conductance due to spin- $\uparrow\downarrow$ scattering, where ρ_{DOS} is the (on-spin) density of state of the electrons in the normal metal, $\frac{N}{s_{sf}}$ is the spin- $\uparrow\downarrow$ relaxation time and V_N the volume of the normal metal node.

The polarization of the source-drain contacts is supposed to be an effective one including the magnetically active region of the bulk ferromagnet with thickness governed by the spin- $\uparrow\downarrow$ diffusion length in the ferromagnet. For the free magnetic layer F3, the perpendicular component of the spin current is absorbed to generate the spin transfer torque. The collinear current has to fulfill the boundary conditions in terms of the chemical potential $\mu_s = \mu_\#$ governed by the diffusion equation

$$\frac{\partial^2 \mu_s^F(z)}{\partial z^2} = -\frac{\mu_s^F(z)}{l_{sd}^F} ; \quad (10)$$

where l_{sd}^F is the spin- $\uparrow\downarrow$ diffusion length in the ferromagnet.

III. SPIN TRANSFER TORQUE AND MAGNETIC FAN EFFECT

In this Section, we solve the Landau-Lifshitz-Gilbert equation including expressions for the spin-transfer torque on the free layer according to the circuit theory sketched above.

A. Currents and spin torque

In metallic structures the imaginary part of the mixing conductance is usually very small and may be disregarded, i.e., $g_i \approx 0$. The source and drain contacts F1 $\uparrow\downarrow$ and F2 $\uparrow\downarrow$ are taken to be identical: $g_1 = g_2 = g$, $p_1 = p_2 = p$ and

$r_1 = r_2 = r$. For F3N we take $r_3 = 3$. In our device, the directions of the magnetization of the fixed magnetic leads are $m_1 = (0; 0; 1)$ and $m_2 = (0; 0; -1)$. For the free layer we allow the magnetization $m_3 = (m_x; m_y; m_z)$ to be arbitrary. We assume that F3 is a coating contact in which the chemical potential μ_0^F adjusts itself such that the net charge current through the interface F3N vanishes:

$$I_c^{(3)} = \frac{eg_3}{2h} [2(\mu_0^F - \mu_0^N) + p_3 \mu_s^F - p_s m_3] = 0: \quad (11)$$

Applying a bias current I_0 on the two ferromagnetic leads, F1 and F2, the conservation of charge current in the normal metal then gives $I_c^{(1)} = I_c^{(2)} = I_0$. At the F3N interface, the continuity of the longitudinal spin current dictates

$$-\sigma \frac{\partial \mu}{\partial z} \Big|_{z=0} - \sigma \frac{\partial \mu}{\partial z} \Big|_{z=0} = \frac{2e^2}{hA} I_{s;3} m_3 \quad (12)$$

where σ (σ) is the bulk conductivities of spin up (down) electrons in the ferromagnet and A the area of the interface. Choosing the origin of the z axis is at the F3N interface and assuming F3 to be of thickness d ,

$$-\sigma \frac{\partial \mu}{\partial z} \Big|_{z=d} - \sigma \frac{\partial \mu}{\partial z} \Big|_{z=d} = 0: \quad (13)$$

With both boundary conditions, the diffusion equation can be solved for the spin accumulation in F3

$$\mu_s^F(z) = \frac{3 \cosh(\frac{z-d}{l_{sd}^F}) s m_3}{3 + \sim \tanh(\frac{d}{l_{sd}^F}) \cosh(\frac{d}{l_{sd}^F})} \quad (14)$$

where $3 = g_3(1 - \beta_s^2) = 4$ characterizes the contact F3N and $\sim = hA \sigma \sigma = (e^2 l_{sd}^F (\sigma + \sigma))$ describes the bulk conduction properties of the free layer with arbitrary m_3 . The limit $l_{sd}^F \rightarrow 0$ corresponds to negligibly small spin-diffusion length, which implies $\tanh(d/l_{sd}^F) \rightarrow 0$. Near the interface, the spin accumulation in F3 then reduces to

$$\mu_s^F = s m_3: \quad (15)$$

In this limit, $I_s^{(3)} m_3 = 0$ the collinear component of the spin current vanishes.

By solving the linear equations generated by Eqs. (8,9), we obtain the spin accumulation s in the normal metal node,

$$s = \hat{C} [\beta_s \vec{T} + W_b] \quad (16)$$

where the elements of the symmetric matrix \hat{C} are given in Appendix A and $W_b = (0; 0; 2phI_0/e)$ is a bias-vector. Eq. (16) contains contribution due to bias current and spin pumping effect. The spin accumulation in the ferromagnet Eq. (14) should be substituted in Eq. (16) to give the spin accumulation in the normal metal, from which the spin transfer torque can be determined according to Eq. (6). For an ultrathin film, the spin transfer torque, including pumping effect and spin accumulation in the ferromagnet, reads,

$$L = \frac{3g_3}{8} \wedge [\beta_s \vec{T} + W_b]; \quad (17)$$

with the elements of \hat{C} listed in Appendix.

B. Dynamics of the free layer

After the bias current is switched on, a spin accumulation builds up in the normal metal. At the beginning, the spin-transfer torque exerted on the magnetization of the free layer (F3) causes a precession out of the plane, hence generating a demagnetizing field H_A that is oriented perpendicular to the film plane. Subsequently the magnetization precesses around H_A and as long as the current I_0 continues, the rotation persists. In order to determine the dynamics of the magnetization, we apply the spin torque term L [Eq. (17)] to the Landau-Lifshitz-Gilbert (LLG) equation (1). Crystalline anisotropies in F3 may be disregarded for soft ferromagnets such as permalloy. The effective field in the LLG equation then reduces to

$$H_A = -\mu_0 M_s (N_x m_x; N_y m_y; N_z m_z); \quad (18)$$

where N_x , N_y and N_z are the demagnetizing factors determined by the shape of the film.²⁷ The anisotropy field keeps the magnetization in the plane when the torque is zero. The spin torque generated by the current bias forces the magnetization out of plane, hence triggering the nearly in-plane rotation of the magnetization. Substituting the spin-torque term Eq. (17) into Eq. (1), we obtain for the following LLG equation,

$$\frac{1}{\gamma} \frac{dm}{dt} = -m \times H_A + \frac{1}{\gamma} (\alpha_0 + \alpha^0) m \frac{dm}{dt} + H_{st}(I_0) \quad (19)$$

Here the last vector

$$H_{st}(I_0) = \frac{h}{2e} \frac{I_0}{M_s V} (\alpha_3 m_x m_z; \alpha_3 m_y m_z; 1 - m_z^2) : \quad (20)$$

is the effective field induced by the spin-transfer torque that depends on the position of the magnetization and the device parameter

$$\alpha_{st} = \frac{p_3 g_3 G_1}{G_t G_3 + 2(p_3^2 - 1 + \alpha) g_3 (1 - m_z^2)}; \quad (21)$$

where G_i 's are introduced in Appendix A. According to Eq. (21), we can accurately engineer the device performance by tuning the conductances and polarizations. Compared with the original LLG equation, a new dimensionless parameter entering the calculation

$$\alpha^0 = \frac{h (Reg^{\#})^2}{2 V M_s} \quad (22)$$

reflects the tensor character of the pumping-induced additional Gilbert damping.²⁸ Choosing contact F3 to be metallic and the others to be tunneling barriers, the condition $g_3 = g; g_{sf}$ can be realized. In that limit α^0 reduces to

$$\alpha^0 = \frac{h}{4 V M_s} Reg_3^{\#}; \quad (23)$$

which agrees with the enhanced Gilbert damping derived in Ref. 22. In the following, we take $\alpha = \alpha_0 + \alpha^0$ to be the enhanced Gilbert damping constant.

1. Vanishing in-plane anisotropy

Here we rewrite the free layer magnetization in two polar angles (in-plane) and (out-of-plane) such that $m = (\cos \theta \cos \phi; \cos \theta \sin \phi; \sin \theta)$ and assuming a small z-component, i.e., $m_z = \sin \theta$ and $\cos \theta \approx 1$. When the free layer is a round flat disk with demagnetizing factors $N_x = N_y = 0$ and $N_z = 1$, the Eqs. (19) reduce to:

$$\begin{aligned} \frac{d\theta}{dt} &= -\frac{d}{dt} \alpha_0 M_s N_z \\ \frac{d\phi}{dt} &= \frac{d}{dt} + F(I_0); \end{aligned} \quad (24)$$

introducing $F(I_0) = h_{st} I_0 / (2e M_s V)$. Eq. (24) separates the motion for the in and out-of-plane angles. We consider the dynamics of a current that is abruptly switched on to a constant value I_0 at $t = 0$, assuming that $\theta(t = 0) = 0$, i.e., a magnetization that initially lies in the plane. The motion of θ for $t > 0$ is then given by

$$\begin{aligned} \theta(t) &= \frac{\alpha^0}{\alpha_0 M_s N_z} (1 - e^{-t/\tau}) \\ \frac{d\phi}{dt} &= \frac{\alpha^0}{1 + \frac{\alpha^0}{\alpha_0}} (1 - e^{-t/\tau}) : \end{aligned} \quad (25)$$

where we introduced the response time

$$\tau = \frac{(1 + \frac{\alpha^0}{\alpha_0})}{\alpha_0 M_s N_z} \quad (26)$$

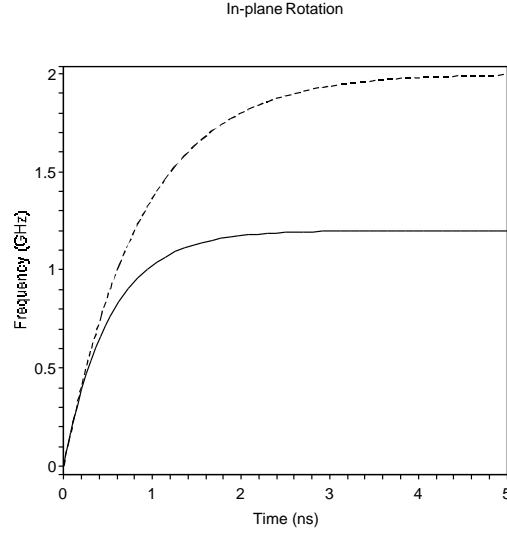


FIG. 2: The in-plane rotation (in the unit of giga hertz) versus time (in nano seconds). The solid line: including spin pumping effect. The dash line: without spin pumping effect.

and the saturation in-plane rotation frequency

$$\omega = \frac{F(I_0)}{2e} = \frac{\hbar}{2e} \frac{I_0}{M_s V} \quad (27)$$

Similarly, the in-plane rotation is governed by

$$\begin{aligned} \omega(t) &= \omega + \frac{\omega}{\omega_0 M_s N_z} (1 - e^{-t/\tau}) \\ \frac{d\omega}{dt} &= \omega + \frac{\omega}{1 + \frac{1}{2}} e^{-t/\tau} \quad (28) \end{aligned}$$

Taking the parameters from Ref. 12, viz. a volume of normal metal $V_n = 400^2 \times 30 \text{ nm}^3$, spin ip time in the normal metal of $\tau_{sf} = 62 \text{ ps}$, density of states $D_{OS} = 2.4 \times 10^{28} \text{ eV}^{-1} \text{ m}^{-3}$, we find $e^2 g_{sf} \hbar = 0.3 \times 10^5$.

Let us take the thickness of the free layer $d = 5 \text{ nm}$. The saturation magnetization of permalloy is $M_s = 8 \times 10^5 \text{ A m}^{-1}$. The relative mixing conductance is chosen $\beta' = 1$ and the bulk value of the Gilbert damping constant for Py is typically $\alpha_0 = 0.006$.²² A metallic interface conductance (for F3N) is typically $1.3 \times 10^6 \text{ m}^{-2}$,²⁹ whereas the source/drain contacts are tunneling barriers with resistance $\hbar = e^2 g = 20 \text{ k}$.¹² The calculated enhancement of the Gilbert damping constant is then $\alpha_0 = 0.004$ and the response time $\tau = 0.52 \text{ ns}$. The motion of the magnetization of the free layer is depicted by Fig. 2 and Fig. 3 for a bias current density of $J = 10^7 \text{ A cm}^{-2}$ with the cross section at the electronic transport direction $400 \times 30 \text{ nm}^2$.¹²

The spin pumping effect through the enhanced Gilbert damping constant reduces the saturation frequency from 2.0 to 1.2 GHz, but also the response time to reach the saturation value from 0.37 to 0.52 ns. Notice that the frequency is directly proportional to I_0 and thus in the absence of any in-plane anisotropy the frequency can be tuned continuously to zero by decreasing the bias current. The out-of-plane motion is very slow compared to the in-plane one: it decreases from 12 MHz to around 0 when the in-plane rotation approaches the saturation frequency. As shown in Fig. 4, within a long period the small angle approximation still holds. A larger ratio of $g_3 = g$ also gives higher frequencies. Decreasing the diameter, and thus also the volume, of the free layer gives a smaller demagnetizing factor N_z , which causes larger a response time according to Eq. (26) and increases the saturation value of the in-plane rotation frequency ω .

2. In-plane anisotropy

In reality, there are always residual anisotropies or pinning centers. Shape anisotropies can be introduced intentionally by fabrication of elliptic F3 discs. We consider the situation in which the free layer is slightly pinned in the plane by an anisotropy field that corresponds to an elliptic (pancake) shape of the ferromagnet. At equilibrium, the

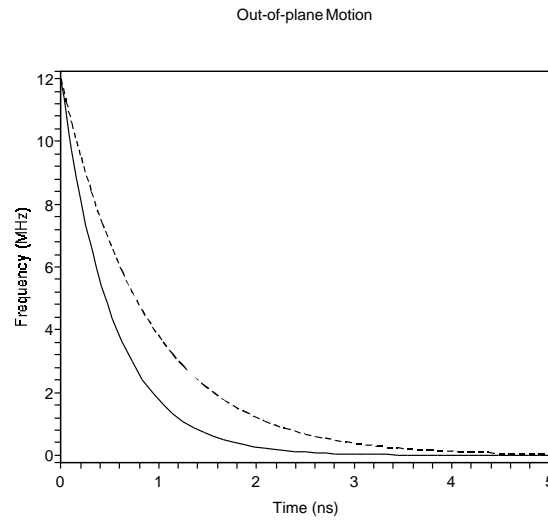


FIG . 3: The out-of-plane motion (in the unit of mega hertz) versus time (in nano seconds). The solid line: including spin pumping effect. The dash line: without spin pumping effect.

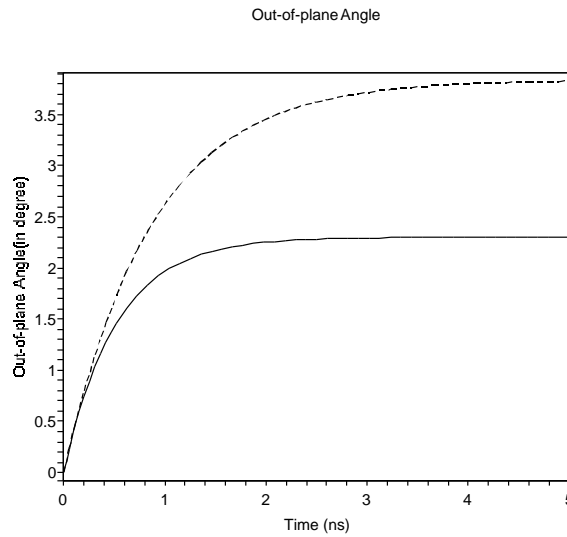


FIG . 4: The out-plane angle (in degree) versus time (in nano seconds). The solid line: including spin pumping effect. The dash line: without spin pumping effect.

For magnetization is then aligned along the easy, let us say, x axis. The in-plane rotation can be sustained only when the spin transfer torque overcomes the effective field generated by the shape anisotropy, hence a critical current I_c for the steady precession is expected. For an ellipse with long axis of 200 nm, thickness 5 nm and aspect ratio 0.9, the two demagnetizing factors are calculated to be $N_y = 0.0224$ and $N_x = 0.0191$. With a Gilbert damping constant $\alpha = 0.01$, the numerical simulation gives $I_c = 4.585$ mA corresponding to a current density $J_c = 3.8 \times 10^7$ A cm⁻² (the cross section is 400 × 30 nm²).¹²

These critical current densities are of the same order of magnitude as those used to excite the magnetization in spin-valve pillars. So even a relatively small anisotropy can cause a significant critical current. In order to operate the magnetic fan at small current densities, the magnetic island should be fabricated as round as possible. The magnetization responds to a current step function below the critical value by damped in-plane and out-of-plane oscillations and comes to rest at a new in-plane equilibrium angle θ_e with zero out-plane component (cf. Figs. 5 and 6). At the steady state, the spin-transfer torque is balanced by the torque generated by the in-plane anisotropy, i.e. the angle θ_e is determined by $\sin(2\theta_e) = 2F(I_0) = (\mu_0 M_s (N_y - N_x))$. With given bias current, smaller $N_y - N_x$ correspond to larger in-plane angles θ_e . According to the theory of differential equations,³⁰ the frequency for the damped magnetization oscillation can be found by diagonalizing the LLG equation at the "equilibrium point" given

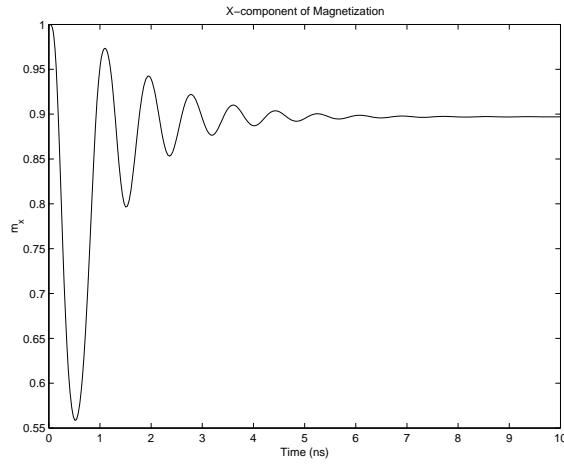


FIG . 5: Below critical current, the x-component of magnetization versus time (in nano seconds). The bias current is 4.5 mA .

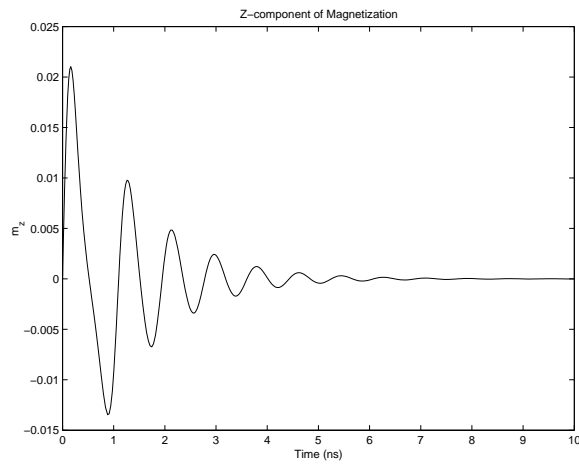


FIG . 6: Below critical current, the z-component of magnetization versus time (in nano seconds). The bias current is 4.5 mA .

by ω_e , this leads to

$$\omega^< = \frac{\mu_0 M_s}{2} \frac{\alpha}{(2N_z - N_x - N_y) \sqrt{D(I_0) + D(I_0)}} ; \quad (29)$$

where

$$D(I_0) = (N_y - N_x)^2 - \frac{4F(I_0)^2}{\mu_0 M_s^2} ; \quad (30)$$

Equation (29) teaches us that below the critical current, decreasing the current increases the rotation frequency. Changing the damping constant does not change $\omega^<$ for a given current but only changes the response time to reach the new equilibrium .

As shown by Fig. 7 to Fig. 9 the magnetization above the critical current saturates into a steady precessional state accompanied by an oscillation of the z-component (nutation). In this situation, ω_e is no longer a constant of motion. Instead the new steady state is given by $m_x = m_y = 0$ and $m_z = F(I_0) = (\mu_0 M_s N_z)$. Diagonalizing the LLG around this point we derive the in-plane rotation frequency

$$\omega^> = \frac{F(I_0)}{N_z} \frac{\alpha \sqrt{(N_z - N_x)(N_z - N_y)}}{N_z} ; \quad (31)$$

In the limit of vanishing in-plane anisotropy, i.e., $N_x = 0$ and $N_y = 0$, we recover the previous result. As shown by

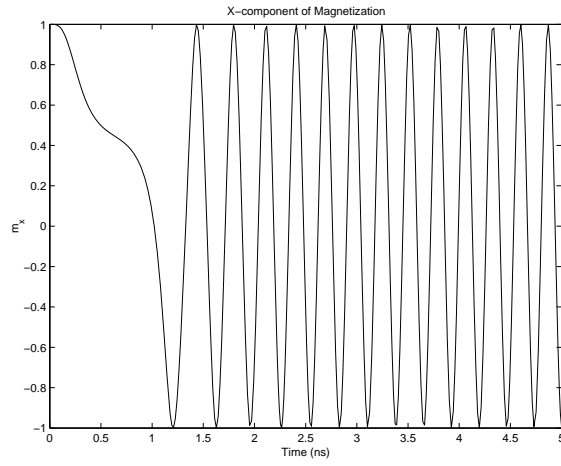


FIG . 7: Above the critical current, the x-component of magnetization versus time (in nano seconds). The bias current is 4.6 mA. The frequency is about 3.6 GHz.

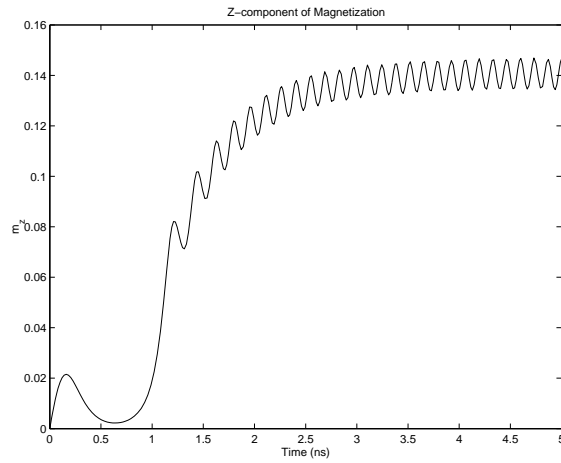


FIG . 8: Above critical current, the z-component of magnetization versus time (in nano seconds). The bias current is 4.6 mA.

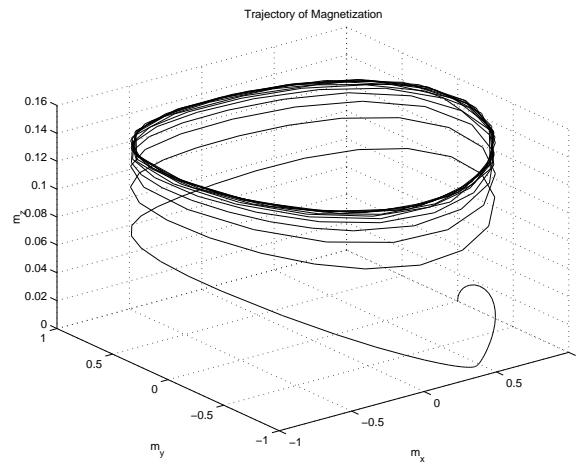


FIG . 9: Above critical current, the trajectory of magnetization within 5 nano seconds. The bias current is 4.6 mA. This picture clearly shows the steady precession of the magnetization.

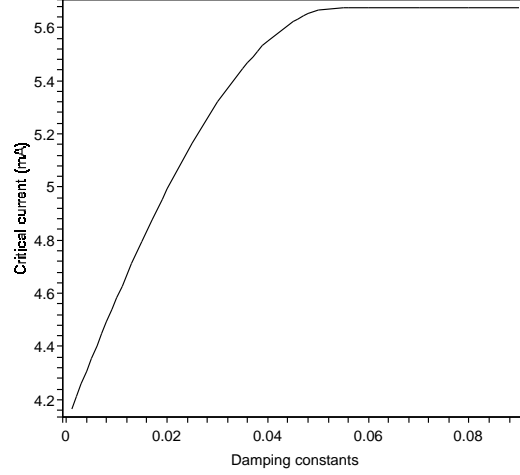


FIG .10: The critical current I_c versus damping constant . This figure shows saturation of I_c above a critical .

Fig. 10, the dependence of the critical current on the damping constant is different from the simple proportionality predicted for pillar structures.⁸ Specifically we observe saturation of the critical current above a critical damping.

In the anisotropic case the extra power necessary for maintaining the motion generates microwaves,^{5,6} which may be attractive for some applications.

IV . A P P L I C A T I O N S

Our "magnetic fan" has the advantage that the magnetization dynamics is not hidden within the structure as in the pillars, but is open to either studies of the dynamics by fast microscopy, or to the utilization of the dipolar field from the soft magnetic island. We envisage applications as magnetic actuators for nanomechanical cantilevers and nanoscale motors, as nanoscale mixers of biological or biomedical suspensions containing magnetic nanoparticles, or as magnetic resonance detectors, again possibly useful for biomedical applications.

A . A c t u a t o r s

The rotating magnetization of the "magnetic fan" generates a periodic dipolar field which can be applied to actuate a nanomechanical cantilever with a (hard) ferromagnetic tip. Assuming for simplicity that the magnet F3 and the cantilever are at a sufficiently large distance the force on the cantilever magnet is given by

$$F = V_c r (M_c - H_d) ; \quad (32)$$

where M_c is the saturation magnetization and V_c is the volume of the cantilever magnet and the field H_d generated by a magnetic dipolar at the position r can be written as

$$H_d = \frac{3(M_c r)r - M_c^2 r}{r^5} ; \quad (33)$$

Assume a cantilever on top of the magnetic fan at a distance of 125 nm (along z-direction),³¹ with beam plane parallel to the plane of the Py film F3 and magnetization along the x-axis. The saturation value of cantilever magnetization is taken as 1.27×10^6 A m⁻¹. Assuming a lateral size of the cantilever magnet³¹ of 150×150 nm² with thickness 50 nm, the force is estimated to be

$$F = 1.1 \times 10^{-8} \cos(\omega t) N \quad (34)$$

where ω is the rotation frequency of the "magnetic fan". To efficiently generate the mechanical modes of the cantilever, the cantilever magnet should be hard enough.

Fixing other parameters, the force scales like $1/r^4$ with respect to distance r . When the two ferromagnets are closer to each other the distribution of the magnetizations increases the force over the value estimated above. We see that in the dipole approximation, the force is already quite significant and it will be significantly larger when the full magnetostatic energy is computed.

Generally, the torque on the cantilever may generate both flexural and torsional motion on the cantilever. The torsional motion coupled to the magnetization dynamics has been investigated for such a system³² and the nanomechanical magnetization reversal based on the torsional modes has been proposed.³³ The coupling of a cantilever to the oscillating dipolar field will be discussed elsewhere.

B. Mixers

The dipolar field produced by our device can also be used to function as mechanical mixer for suspensions of magnetic particles. To this end we should scale down the frequency of the rotating magnetization either by decreasing the bias current or re-engineering the parameters of the device, e.g., increasing the thickness of the Py film. Low saturation magnetization is detrimental in this case, since that would also reduce the usable stray fields. By these ways, one hopefully can access the kilohertz frequency region, which is important for the hydrodynamic motion in ferrofluids.³⁴

C. Detectors

An external field tunes the frequency of the rotation of the magnetization. Response to the change of the frequencies is the rebuilding of the spin accumulation in the normal metal hence altering the source-drain resistance R_{SD} . Due to the relation

$$\frac{F_0^1}{0} \frac{F_0^2}{0} = R_{SD} I_0 ; \quad (35)$$

this deviation is reflected on the source-drain voltage-current curve. This feature can be implemented as a sensor for biomedical applications in order to detect the presence of magnetic beads, which are used as labels in biosensors.³⁵ Furthermore, the ability to change the frequency of the "magnetic fan" should allow to measure locally the frequency dependence of the magnetic susceptibility, which offers an alternative pathway to using magnetic nanoparticles for biosensing applications.^{36,37}

V. CONCLUSION

We studied the magnetization dynamics of a magnetic transistor, i.e., a lateral spin valve structure with perpendicular-to-plane magnetizations and an in-plane free layer attached to the normal metal that is excited by an external current bias. By circuit theory and the Landau-Lifshitz-Gilbert equation, analytic results were obtained for the spin-transfer torque and the dynamics of the magnetization in the limit of small out-of-plane angle. Spin precession and spin pumping effects were also investigated analytically and an anisotropic enhanced Gilbert damping was derived for the free layer magnetization. Without an externally applied magnetic field, a continuous rotation of the magnetization of the free layer at GHz frequencies can be achieved. In the lateral geometry, the free layer is no longer buried or penetrated by a dissipating charge current, thus becomes accessible for more applications. Our methods handle the microscopic details on crucial issues like spin-torque transfer efficiency, spin-precession scattering and the response time, hence offering accurate design and control. The rotation can be observed, e.g., by magneto-optical methods. This new device has potential applications as high frequency generator, actuator of nanomechanical systems, biosensors, and other high-speed magnetoelectronic devices.

Acknowledgments

We thank Yu. V. Nazarov, J. Slonczewski and A. Kovalev for fruitful discussions. X. Wang acknowledges H. Saarikoski's help with the preparation of the manuscript. This work is supported by NanoNed, the FOM, U.S. Department of Energy, Basic Energy Sciences, under Contract No. W-31-109-ENG-38 and the EU Commission FP6 NMP-3 project 505587-1 "SFINX". GEWB would like to acknowledge the support through the Materials Theory Institute and the hospitality he enjoyed at Argonne.

APPENDIX A: SPIN ACCUMULATION IN NORMAL METAL NODE

Here we summarize a number of complex angle dependent coefficients. The elements of the symmetric matrix \hat{C} in Eq.(16) read

$$C_{11} = \frac{G_t (G_1 - G_4 m_x^2) - 2g(p^2 - 1 +) (G_t - G_4 m_y^2)}{Q} \quad (A 1)$$

$$C_{12} = C_{21} = \frac{G_2 G_4 m_x m_y}{Q}; \text{ and } C_{13} = C_{31} = \frac{G_t G_4 m_x m_z}{Q} \quad (A 2)$$

$$C_{22} = \frac{G_2 (G_t - G_4 m_x^2) - G_t G_4 m_z^2}{Q} \quad (A 3)$$

$$C_{23} = C_{32} = \frac{G_t G_4 m_y m_z}{Q}; \text{ and } C_{33} = \frac{G_t (G_1 + G_4 m_z^2)}{Q} \quad (A 4)$$

introducing

$$G_1 = (1 - p^2)(1 - g_3)g_3 + 2g + 2g_{sf} \quad (A 5)$$

$$G_2 = -g_3 g_3 + 2(1 - p^2)g + 2g_{sf} \quad (A 6)$$

$$G_3 = (1 - p^2)(1 - g_3)g_3 + 2(1 - p^2)g + 2g_{sf} \quad (A 7)$$

$$G_4 = -g_3 g_3 - (1 - p^2)(1 - g_3)g_3 \quad (A 8)$$

$$G_t = -g_3 g_3 + 2g + 2g_{sf} \quad (A 9)$$

$$Q = G_t [G_t G_3 + 2(p^2 - 1 +)gG(1 - m_z^2)] \quad (A 10)$$

$$g_3 = \frac{3}{3 + \sim \tanh(d=l_{sd}^F)}; \quad (A 11)$$

in the limit of negligible spin flip in F, i.e., $d \ll l_{sd}^F$, then $g_3 \rightarrow 1$. The elements of the matrix in Eq.(17) are given by

$$C_{11} = \frac{G_t G_3 (1 - m_x^2) + 2G_4 (p^2 - 1 +)gm_y^2}{Q} \quad (A 12)$$

$$C_{12} = C_{21} = \frac{G_t G_2 m_x m_y}{Q}; \text{ and } C_{13} = C_{31} = \frac{G_t G_1 m_x m_z}{Q} \quad (A 13)$$

$$C_{22} = \frac{G_t G_3 (1 - m_y^2) + 2G_4 (p^2 - 1 +)gm_x^2}{Q} \quad (A 14)$$

$$C_{23} = \frac{G_t G_1 m_y m_z}{Q}; \text{ and } C_{31} = \frac{G_t G_3 m_x m_z}{Q} \quad (A 15)$$

$$C_{32} = \frac{G_t G_3 m_y m_z}{Q}; \text{ and } C_{33} = \frac{G_t G_1 (1 - m_z^2)}{Q} \quad (A 16)$$

¹ J.C.Slonczewski, J.Magn.Magn.Mater. 159, L1 (1996).

² L.Berger, Phys.Rev.B 54, 9359 (1996).

³ J.A.Katine, F.J.Albert, R.A.Buhrman, E.B.Myers, and D.C.Ralph, Phys.Rev.Lett. 84, 3149 (2000).

⁴ E.B.Myers, F.J.Albert, J.C.Sankey, E.Bonet, R.A.Buhrman, and D.C.Ralph, Phys.Rev.Lett. 89, 196801 (2002).

⁵ S.I.Kiselev, J.C.Sankey, I.N.Kivorotov, N.C.Emley, R.J.Schoelkopf, R.A.Buhrman, and D.C.Ralph, Nature (London) 425, 380 (2003).

⁶ W.H.Rippard, M.R.Pufall, S.Kaka, S.E.Russek, and T.J.Silva, Phys.Rev.Lett. 92, 027201 (2004).

⁷ A.Kent, B.Ozyilmaz, and E.delBarco, App.Phys.Lett. 84, 3897 (2004).

⁸ K.J.Lee, O.Redon, and B.Dieny, App.Phys.Lett. 86, 022505 (2005).

⁹ H.Xi, K.Z.Gao, and Y.Shi, J.Appl.Phys. 97, 044306 (2005).

- ¹⁰ F. J. Jedema, A. T. Filip, and B. J. van Wees, *Nature* 410, 345 (2001).
- ¹¹ F. J. Jedema, H. B. Heersche, A. T. Filip, J. J. A. Baselmans, and B. J. van Wees, *Nature* 416, 713 (2002).
- ¹² M. Zaanen and B. J. van Wees, *Phys. Rev. Lett.* 91, 186601 (2003).
- ¹³ T. Kinura, J. Hamrle, Y. Otani, K. Tsukagoshi, and A. Aoyagi, *App. Phys. Lett.* 85, 3501 (2004).
- ¹⁴ S. O. Valenzuela and M. Tinkham, *App. Phys. Lett.* 85, 5914 (2004).
- ¹⁵ Y. Ji, A. Homann, J. S. Jiang, and S. D. Bader, *App. Phys. Lett.* 85, 6218 (2004).
- ¹⁶ G. E. W. Bauer, A. Brataas, Y. Tserkovnyak, and B. J. van Wees, *App. Phys. Lett.* 82, 3928 (2003).
- ¹⁷ E. Saitoh, H. Miyajima, T. Yamaguchi, and G. Tatara, *Nature (London)* 432, 203 (2004).
- ¹⁸ J. Grollier, M. V. Costache, C. H. van der Wal, and B. J. van Wees, *cond-mat/0502197* (2005).
- ¹⁹ T. Kinura, Y. Otani, and J. Hamrle, *cond-mat/0508559* (2005).
- ²⁰ A. Brataas, Y. V. Nazarov, and G. E. W. Bauer, *Phys. Rev. Lett.* 84, 2481 (2000).
- ²¹ P. F. Carcia, *J. Appl. Phys.* 63, 5066 (1988).
- ²² Y. Tserkovnyak, A. Brataas, and G. E. W. Bauer, *Phys. Rev. Lett.* 88, 117601 (2002).
- ²³ Y. Tserkovnyak, A. Brataas, G. E. W. Bauer, and B. I. Halperin, *cond-mat/0409242* (2004).
- ²⁴ I. N. Kivorotov, N. C. Emley, J. C. Sankey, S. I. Kiselev, D. C. Ralph, and R. A. Buhrman, *Science* 307, 228 (2005).
- ²⁵ J. Xiao, A. Zangwill, and M. D. Stiles, *Phys. Rev. B* 72, 014446 (2005).
- ²⁶ A. Brataas, Y. V. Nazarov, and G. E. W. Bauer, *Eur. Phys. J. B* 22, 99 (2001).
- ²⁷ J. A. Osborn, *Phys. Rev.* 67, 351 (1945).
- ²⁸ X. Wang and G. E. W. Bauer, unpublished (2004).
- ²⁹ A. Kovalev, G. E. W. Bauer, and A. Brataas, *cond-mat/0504705* (2005).
- ³⁰ L. Perko, *Differential Equations and Dynamical Systems* (Springer, Berlin, 1996), 2nd ed.
- ³¹ D. Rugar, R. Budakian, H. J. Mamin, and B. W. Chui, *Nature* 430, 329 (2004).
- ³² A. A. Kovalev, G. E. W. Bauer, and A. Brataas, *App. Phys. Lett.* 83, 1584 (2003).
- ³³ A. A. Kovalev, G. E. W. Bauer, and A. Brataas, *Phys. Rev. Lett.* 94, 167201 (2005).
- ³⁴ M. I. Shliomis and V. I. Stepanov, *Adv. Chem. Phys.* 87, 1 (1994).
- ³⁵ D. R. Baselt, G. U. Lee, M. Natesan, S. W. Metzger, P. E. Sheehan, and R. J. Colton, *Biosens. Bioelectron.* 13, 731 (1998).
- ³⁶ J. Connolly and T. G. St Pierre, *J. Magn. Magn. Mater.* 225, 156 (2001).
- ³⁷ S. H. Chung, A. Homann, S. D. Bader, C. Liu, B. Kay, L. Makowski, and L. Chen, *App. Phys. Lett.* 85, 2971 (2004).